nature geoscience

Article

https://doi.org/10.1038/s41561-025-01792-3

A shift from human-directed to undirected wild land disturbances in the USA

Received: 13 December 2024

Accepted: 15 August 2025

Published online: 18 September 2025

Check for updates

Shi Qiu[1] ✉, Zhe Zhu[1] ✉, Xiucheng Yang[1], Curtis E. Woodcock[2], Robert T. Fahey[1,3], Stephen Stehman[4], Yingtong Zhang[2], Mari Cullerton[1], Ashley Grinstead[1], Falu Hong[1], Kexin Song[1], Ji Won Suh[1], Tian Li[1], Wei Ren[1] & Ramakrishna R. Nemani[5]

Land disturbances are fundamental drivers of terrestrial ecosystem dynamics, influencing biodiversity, carbon cycling and land–atmosphere interactions. An understanding of changes in their regimes is crucial for predicting future ecosystem trajectories and guiding sustainable land management. Here we leverage the long-term record of Landsat imagery to create high-resolution (30 m) maps of annual land disturbance agents across the contiguous USA from 1988 to 2022. We find that 178.50 million hectares of US land have been cumulatively disturbed over this period. Human-directed disturbances account for 65% of this total, driven by logging, agricultural disturbance and construction. Our analysis reveals a widespread decline in human-directed disturbances (−59.21 kha yr^{-1}) alongside a countervailing surge (20.31 kha yr^{-1}) in less controllable, undirected 'wild' disturbances (fire, wind/geohazard and vegetation stress), which account for 24% of the total disturbed area. The disturbance regime shift analysis finds that although human-directed disturbances are now declining in frequency, wild disturbance frequencies are increasing at an accelerated pace. The patch size of human-directed disturbances is shrinking, while the wild disturbance patch size shows both expanding and contracting trends. Disturbance severity is rising across most of the USA. Our findings highlight an urgent need to understand and adapt to these diverging disturbance trajectories, as they will profoundly shape the future of US landscapes.

Land disturbances are a primary architect of Earth's terrestrial ecosystems, shaping their patterns, processes and resilience. These disturbance events affect the natural world and human societies through effects on resource availability, natural hazards and climate change[1]. Historically, two distinct narratives have shaped our understanding of disturbance. One describes nature's raw power: wildfires ignited by lightning; hurricanes reshaping coastlines; pest outbreaks transforming forests. These natural disturbances have been agents of change for millennia, integral to the evolution and dynamics of ecosystems[2]. The other narrative chronicles the rise of human impact. Over the past century, anthropogenic disturbances such as logging, agricultural disturbance and construction have intensified, leaving a pervasive footprint on Earth's ecosystems[3–7].

However, these two tales are now intertwined. Human actions are altering natural disturbance regimes, blurring the lines between 'natural' and 'anthropogenic'. This blurring is driven not only by direct

[1]Department of Natural Resources and the Environment, University of Connecticut, Storrs, CT, USA. [2]Department of Earth and Environment, Boston University, Boston, MA, USA. [3]Center for Environmental Sciences and Engineering, University of Connecticut, Storrs, CT, USA. [4]College of Environmental Science and Forestry, State University of New York, Syracuse, NY, USA. [5]Bay Area Environmental Research Institute, NASA Ames Research Center, Moffett Field, CA, USA. ✉e-mail: shi.qiu@uconn.edu; zhe@uconn.edu

interventions such as prescribed burning or dam construction but also by the indirect effects of anthropogenic climate change[8], which could amplify the frequency, size and severity of many natural disturbances. For example, rising global temperatures are contributing to more intense hurricanes[9], prolonged droughts[10] and expanded ranges of forest pests[11]. These changes, in turn, are contributing to a surge in what we term undirected 'wild' disturbances—those agents of change, including fire, wind/geohazard and stress, that can be associated with either natural or anthropogenic sources, but are largely not explicitly directed by human actions. Water disturbance is associated with both direct human interventions (for example, dams and reservoirs) and natural events (for example, precipitation and sea level rise) and is thus treated as a distinct category, recognizing its dual drivers.

This convergence of intensifying human impacts and less controllable wild disturbances creates a complex and rapidly changing disturbance landscape, making it crucial to understand not just individual disturbance events, but also the broader context of disturbance regimes—the cumulative effect of multiple disturbances across space and time[12]. Disturbance regimes, characterized by their frequency, size and severity, profoundly influence ecosystem structure and function, shaping their response to change[13].

However, mapping and quantifying disturbance regimes at the needed scale and resolution, particularly for different causal agents, remains a challenge[14]. While research has illuminated shifts in specific disturbance agents and their potential consequences[15–18], a comprehensive understanding of these shifts across diverse drivers and land surface types remains elusive[19]. This gap is exacerbated by limitations in existing disturbance datasets[20–23], which often lack the spatial detail, temporal depth and agent specificity needed to capture the complexity of US disturbance regimes.

Here we define land disturbance as any relatively discrete event that substantially alters the biophysical state of the land surface, including both natural and anthropogenic drivers[13,24]. Our approach focuses on capturing detectable deviations from baseline conditions or established patterns using satellite observations. Consequently, our analysis includes a broad spectrum of events that fit this definition, such as changes in agricultural practices or constructions in already developed areas, all of which represent detectable changes relevant to landscape dynamics. To investigate these dynamics across the contiguous USA, we created a 35-yr (1988–2022) land disturbance dataset using dense satellite time series, object-based analysis and machine learning (Fig. 1). This dataset allows us to quantify not only the spatial extent of different disturbance agents but also shifting disturbance regimes. It is useful to contrast our focus on land disturbance with the concept of land cover and land use change (LCLUC). LCLUC primarily describes the outcome of change, measured in terms of cover types or land uses (for example, shift from forest to cropland), whereas land disturbance is the driver[19]. Disturbances frequently occur without necessarily altering the LCLUC category (for example, forest stress from drought or pests, shifts in agricultural intensity or fallowing cycles)[19], while LCLUC can sometimes occur without a discrete disturbance event (for example, gradual forest regeneration). For example, agricultural expansion may occur once at a given location, but agricultural disturbance can recur through abandonment, intensification or altered management practices (Extended Data Fig. 1). Our analysis addresses seven major disturbance agents: logging; construction; vegetation stress; agricultural disturbance; wind/geohazard; water disturbance; and fire (Extended Data Table 1).

High-resolution land disturbance agent maps

We leveraged 13.45 million Landsat images to generate a 30-m resolution dataset of annual land disturbance maps across the USA from 1988 to 2022 (Methods), capturing the timing, causal agent and severity (Fig. 1 and Extended Data Fig. 2). This dataset identifies diverse disturbances, such as logging in Arkansas (Fig. 1b), expansion and reconstruction of Chicago O'Hare International Airport (Fig. 1c), crop rotation between corn, cotton and wheat in Texas (Fig. 1d), 2011 severe drought in the southern USA (Fig. 1e), 2017 Irma hurricane in Florida (Fig. 1f), 2020 August Complex fire in California (Fig. 1g) and water disturbance in Malheur Lake (Fig. 1h). Our maps were rigorously validated using a stratified random sample of 907 plots (30 m × 30 m), and the estimated user's and producer's accuracies exceeded 75% for most disturbance agents (Extended Data Table 2). Accuracies for wind/geohazard were lower (about 50%), but their limited extent had minimal impact on overall map accuracy (>99%). Mapped stress captures spectrally detectable events such as moderate-to-severe drought and major pest outbreaks, although more subtle physiological stress may be underestimated.

Disturbance footprint

Across the USA (1988–2022), 18% of the land was disturbed at least once, but the cumulative area affected by repeated disturbances totalled 178.50 million hectares (Mha; 95% confidence interval (CI) 170.76–186.24; Extended Data Table 3), equivalent to roughly one third of the nation's land surface. Human-directed disturbances were the primary driver (65% of the total disturbed area). Logging was the largest component (58.85 Mha; 95% CI 52.70–65.00), followed by agricultural disturbance (43.00 Mha; 95% CI 37.19–48.81) and construction (13.73 Mha; 95% CI 11.74–15.72). Wild disturbances accounted for a growing proportion (24%), dominated by fire (15.40 Mha (95% CI 14.13–16.67)) and stress (24.38 Mha (95% CI 21.25–27.51)), while wind/geohazard contributed a smaller share (2.6 Mha; 95% CI 0.56–4.64; Extended Data Table 3). Water disturbances accounted for the remaining 11% (20.54 Mha (95% CI 17.80–23.28)).

The disturbance footprint is highly variable (Extended Data Fig. 3 and Extended Data Table 3). Regionally, the Southeast was the most heavily disturbed, accounting for 34% (62.49 Mha (95% CI 41.17–83.81)) of the total disturbed area. This is probably a reflection of the region's prominent logging industry[25] as well as its vulnerability to frequent hurricanes[26]. By contrast, the Northeast experienced the least disturbance (3.56 Mha (95% CI 0.21–6.91)).

We also describe geographic patterns of disturbance by illustrating variation across latitudinal and longitudinal gradients (Fig. 1i,j). Disturbances are more extensive in southern latitudes, with more than 75% of the total disturbed area concentrated in the Southeast, Southern Great Plains and Southwest (Extended Data Table 3). While these regions show a mix of human-driven disturbances such as logging and construction, they are also vulnerable to the power of wild forces, such as stress, much of which is probably associated with drought, and wind/geohazard (Fig. 1j). Geographic patterns further highlight a concentration of logging and construction in the East (Fig. 1i). Wind/geohazard disturbances, particularly hurricanes, are clustered along the southeastern coast, while fires are more common in the West. Water and agricultural disturbances show peaks in the central regions.

Diverging human-directed and wild disturbance trends

Temporal trend analysis reveals two contrasting trajectories (Fig. 2). Overall, total disturbed area declined annually (−47.73 kha yr^{-1} (95% CI −20.42 to −81.44)), driven by reductions in logging (−8.14 kha yr^{-1} (95% CI −13.86 to −2.97)), construction (−6.72 kha yr^{-1} (95% CI −9.30 to −3.90)), agricultural disturbance (−43.52 kha yr^{-1} (95% CI −62.84 to −26.34)) and water disturbance (−6.20 kha yr^{-1} (95% CI −10.12 to −1.90)). This decrease of human-directed disturbance areas (−59.21 kha yr^{-1} (95% CI −80.90 to −43.03)) probably reflects policy changes, technological advancements in agriculture and forestry, and economic shifts. The history of US agricultural policy is a prime example. While policies in the 1980s aimed at boosting production and exports, leading to more intensive agricultural activities and potential

https://doi.org/10.1038/s41561-025-01792-3

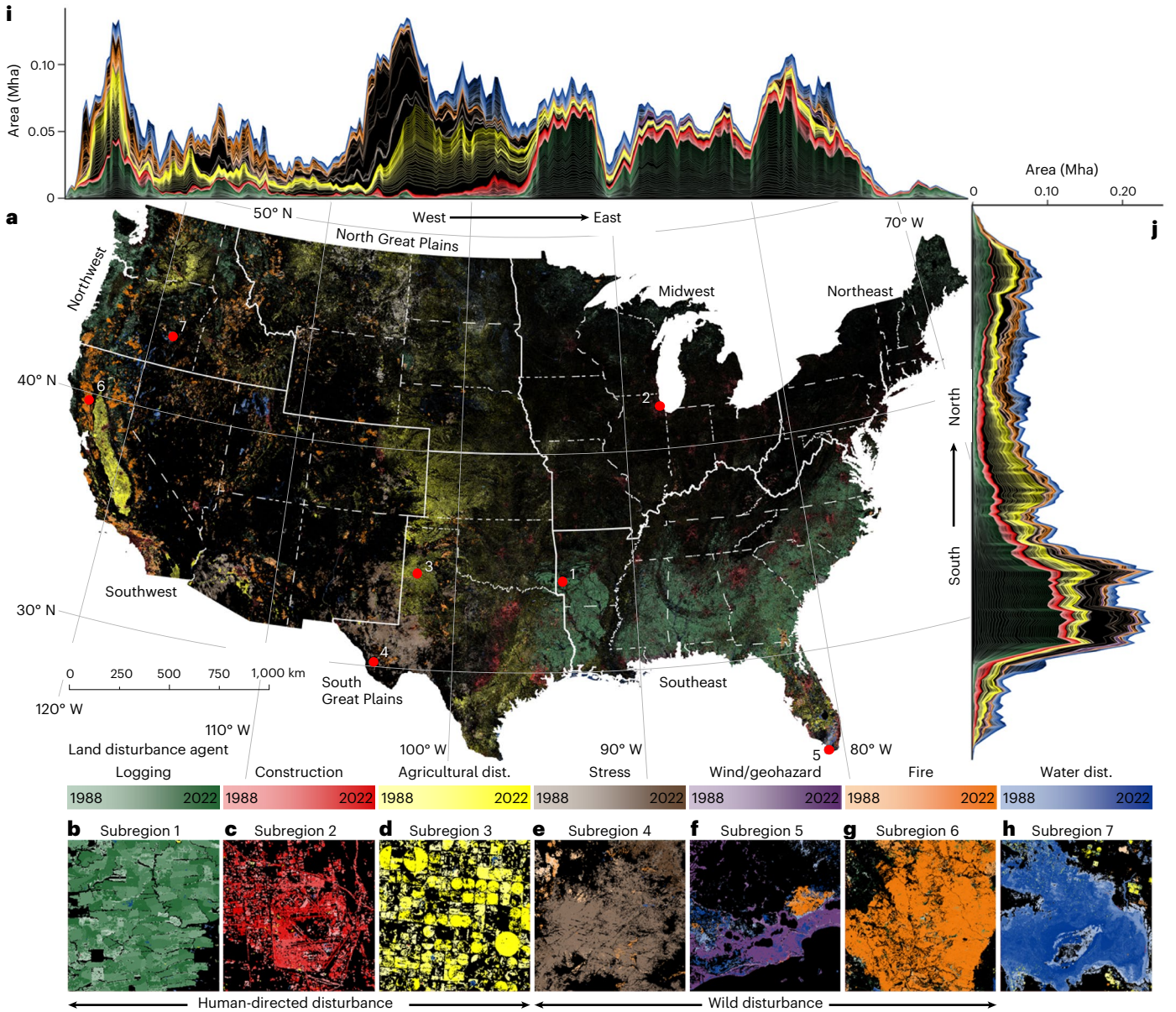

Fig. 1 | Land disturbance agent maps across the USA (1988–2022). a, USA-wide map highlighting each pixel's most recent disturbance agent, revealing the spatial distribution and diversity of disturbances at 30-m resolution. The solid boundaries represent US Fifth National Climate Assessment regions, while the dashed boundaries indicate state borders. **b**–**h**, Examples of disturbance agents from locations 1–7 of the USA include human-directed disturbances (logging (**b**), construction (**c**), agricultural disturbance (dist.; **d**)), wild disturbances (stress (**e**), wind/geohazard (**f**), fire (**g**)) and water disturbance (**h**). The corresponding disturbance severity maps are presented in Extended Data Fig. 2. All maps are shown in Albers equal-area conic projection. **i**,**j**, Longitudinal (**i**) and latitudinal (**j**) profiles overlaid on this projection of stacked disturbance areas. Area statistics (Mha) are calculated at 15-km intervals and stacked chronologically from 1988 to 2022 for different disturbance agents. All panels share the same legend: brighter colour curves represent earlier disturbance years (towards 1988), while darker colours indicate more recent years (towards 2022). Full-resolution maps are available at the interactive explorer https://ee-gers.projects.earthengine.app/view/us-disturbance.

environmental impacts, subsequent Farm Bills emphasized environmental compliance, renewable energy and climate-smart agricultural practices, potentially contributing to the decline in agricultural disturbance we observed. Similarly, the US Lacey Act, amended in 2008 to prevent illegal timber harvesting, probably played a role in reducing logging disturbances. Economically, the 2008 financial crisis clearly affected construction, which has not returned to pre-crisis levels despite recovery (Fig. 2c).

By contrast, we see a significant increase in wild disturbance areas (20.31 kha yr^{-1} (95% CI 1.97–35.65); Fig. 2a), with fire, stress and wind/geohazard exhibiting increasing trends (Fig. 2e–g). This rise is probably driven by climate change, altered fire regimes[27] and other environmental factors. The increase in fire (11.24 kha yr^{-1} (95% CI 3.90–23.54)) is particularly pronounced, reflecting the growing influence of climate change and its interaction with drought, pest outbreaks and historical fire suppression on wildfire activity across the western USA, coupled with evolving fire management strategies[28]. Stress-related disturbances show considerable interannual variability, with peaks linked to major drought events (for example, 2012)[29], and exhibit a non-statistically significant, increasing trend overall (0.61 kha yr^{-1} (95% CI −3.96–10.64), $P = 0.82$). Similarly, wind/geohazard disturbances have increased (0.95 kha yr^{-1} (95% CI 0.00–1.64), $P = 0.06$), potentially reflecting the

https://doi.org/10.1038/s41561-025-01792-3

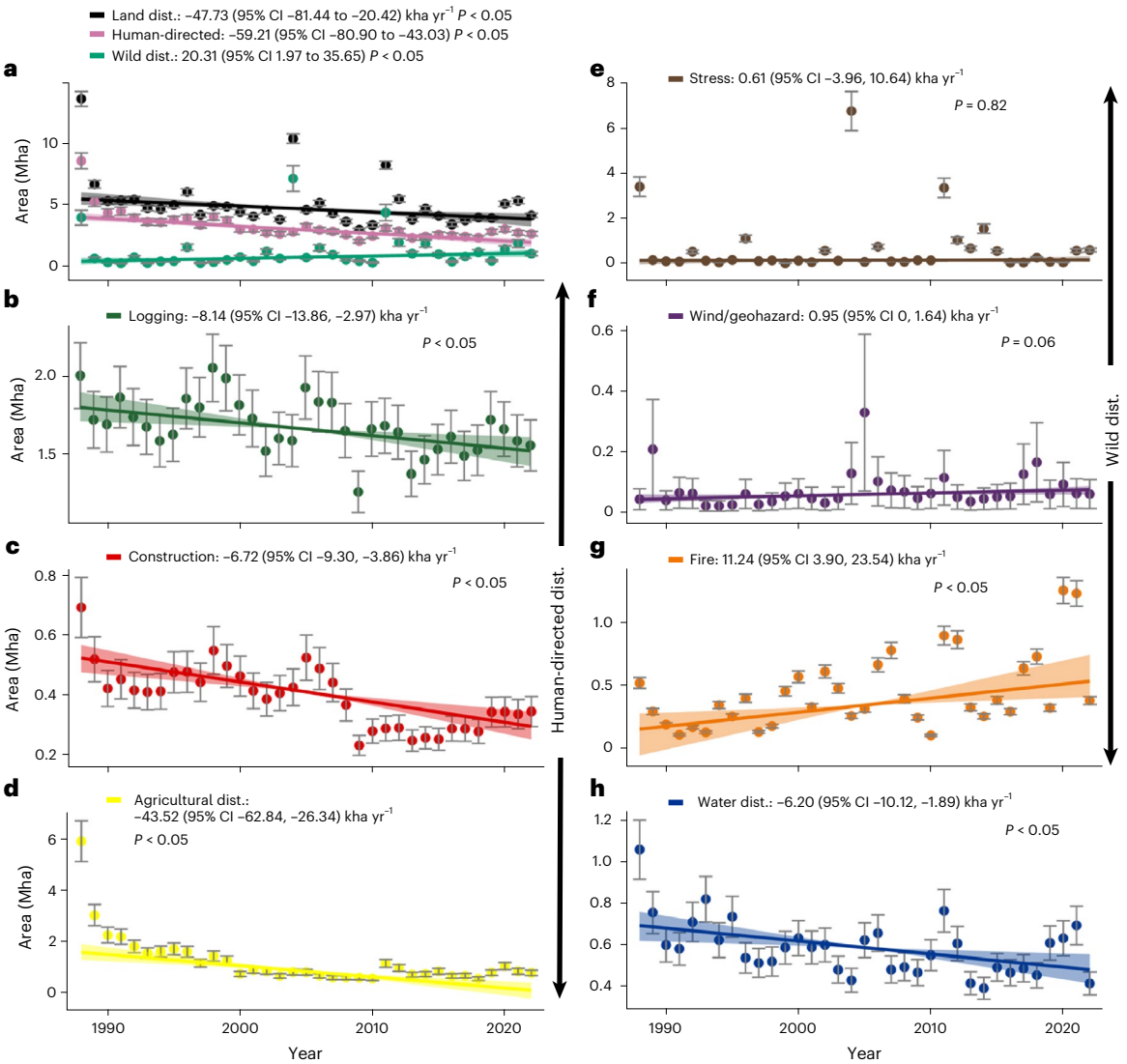

Fig. 2 | Temporal trajectories of land disturbances across the USA (1988–2022). **a**, Temporal trends in annual disturbed area for total land disturbance ($P = 0.00377$), human-directed disturbance ($P < 0.00001$) and wild disturbance ($P = 0.02484$). **b**–**h**, Temporal trends for logging ($P = 0.00196$; **b**), construction ($P = 0.00006$; **c**), agricultural disturbance ($P < 0.00001$; **d**), stress ($P = 0.82025$; **e**), wind/geohazard ($P = 0.06085$; **f**), fire ($P = 0.00697$; **g**) and water disturbance ($P = 0.06085$; **h**). Trends (kha yr^{-1}) estimated using the Theil–Sen estimator, with 95% CIs (shaded areas) and *P* values derived from the two-tailed Mann–Kendall test (Methods). Solid points represent the annual unbiased disturbance area, and the grey error bars indicate the 95% CI based on the validation dataset (Extended Data Table 2).

rise in extreme weather[30]. These contrasting trends underscore a major shift in the drivers of land disturbance across the USA.

Land disturbance regimes

US disturbance regimes vary widely in frequency, size and severity (Fig. 3). The annual average frequency of land disturbance at the landscape scale (hexagonal grid) is 0.36 patches per square kilometre per year, with the top 1% reaching 1.63 patches per square kilometre (Extended Data Table 4). Hotspots of intense, recurring disturbance (>1 patch per square kilometre per year) emerge in agricultural regions of California, Washington State and the Southern Great Plains, driven by dynamic agricultural systems (Extended Data Fig. 4a (3)). The Southeast also experienced a high frequency of disturbances, primarily from logging, wind/geohazard (for example, hurricanes) and water disturbance (Extended Data Fig. 4a (1, 5 and 7)). Across the USA, human-directed disturbances and water disturbance are generally more frequent than the other three wild disturbance categories (Extended Data Fig. 4a and Extended Data Table 4). However, in parts of the Northeast, Midwest and Northwest, lower disturbance frequencies point to relatively more stable ecosystems (Fig. 3a).

The size of disturbance patches across the USA reveals a large contrast between human-directed and wild disturbance (Fig. 3b). While the average disturbance size spans 2.51 hectares (ha), wild disturbances—notably stress (16.82 ha) and fire (10.72 ha)—carve out substantially larger areas per event than human-directed disturbances such as logging (3.06 ha) or construction (1.24 ha; Extended Data Table 4), a pattern particularly pronounced in the western USA. While smaller disturbance patches dominate the East, considerable variation exists (Fig. 3b). For example, logging and wind/geohazard (for example, hurricanes) contribute to larger patch sizes in the Southeast, reflecting the region's forest management practices and susceptibility to major storms (Extended Data Fig. 4b (1 and 5)).

The severity of land disturbance, ranging from 1 (low) to 4 (very high), varies markedly (Fig. 3c). The average severity is 2.51 (between medium to high; Extended Data Table 4), with high-average-severity disturbance hotspots in the central regions where multiple agents

https://doi.org/10.1038/s41561-025-01792-3

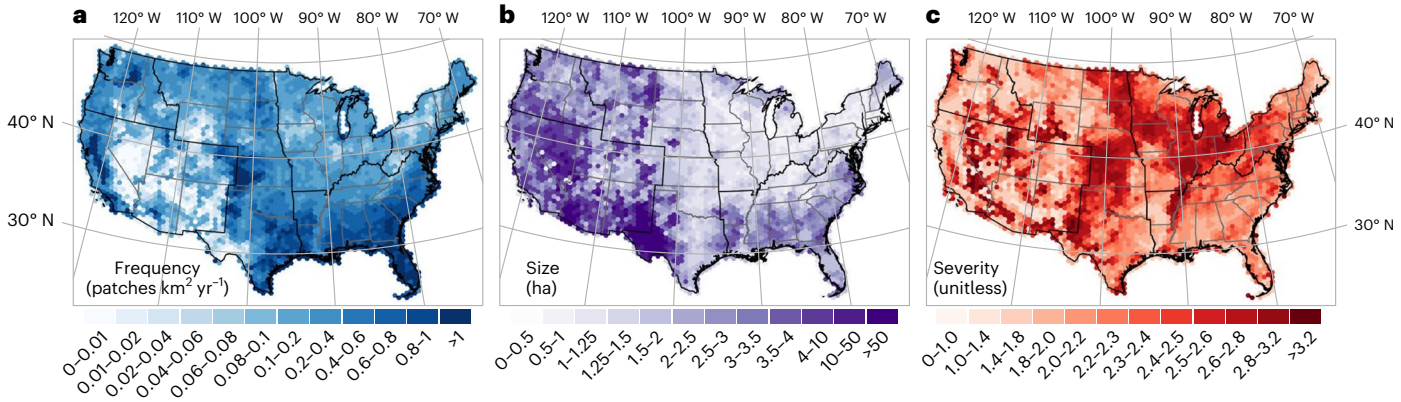

Fig. 3 | Land disturbance regimes across the USA represented in 2,500-km^2 hexagonal grids (1988–2022). a, Average disturbance patch frequency. **b**, Average disturbance patch size. **c**, Average disturbance patch severity, scaled from 1 to 4, where 0–1 indicates undisturbed to low, 1–2 indicates low to medium, 2–3 indicates medium to high, and 3–4 indicates high to very high. All maps are shown in Albers equal-area conic projection. The black boundaries represent US Fifth National Climate Assessment regions, while the grey boundaries indicate state borders. The consistent colour scale across all maps facilitates direct comparison of regime characteristics across different disturbance agents. Each individual disturbance agent regime for logging, construction, agricultural disturbance, stress, wind/geohazard, fire and water disturbance is provided in Extended Data Fig. 4. Histograms corresponding to each map are provided in Supplementary Fig. 6.

converge (Extended Data Fig. 4c (1–4 and 6)). Fire severity is especially prominent in the South Great Plains, Midwest and Southeast (Extended Data Fig. 4c (6)). Wind/geohazard also contributes to high severity in the central regions and along the hurricane-prone eastern coast (Extended Data Fig. 4c (5)). Higher-severity water disturbances are prevalent in most regions except for the Southeast (Extended Data Fig. 4c (7))

Shifting and diverging disturbance regime

Our analysis reveals a dynamic landscape of disturbance regimes (Fig. 4). While overall disturbance frequency declined between 1988 and 2022 (56% of hexagonal grids exhibiting significantly negative trends and 4% showing significantly positive trends; Fig. 4a and Extended Data Table 5), the story is far from uniform. The overall decline is primarily driven by reduction in human-directed and water disturbances (Extended Data Table 5). This pattern suggests that policy changes aimed at promoting more sustainable land management practices, as well as technological advancements and economic shifts, may be having a measurable effect. Most of these declining trends are also decelerating (see density plot in Fig. 4a), further hinting at a potential stabilization of human-directed and water disturbance regimes in some regions. However, this trend is counterbalanced by a rapid surge in wild disturbance. Wind/geohazard, stress and fire all show accelerating increases in disturbance frequency, with hotspots concentrated in the Midwest and West (Extended Data Fig. 5a (4–6)). This accelerating rise in wild forces, particularly fire, points to the growing influence of less controllable forces, posing a challenge for land management and conservation. Wind/geohazard disturbances, particularly hurricanes, exhibit the most pronounced increases in frequency along the Southeast coast, underscoring the region's vulnerability to increasingly frequent and intense storms.

The size of disturbance patches also exhibits non-stationarity, with 30% of hexagonal grids showing statistically significant temporal trends. About half of these grids showed positive trends while the other half showed negative trends (Fig. 4b and Extended Data Table 5). Larger disturbance patches are becoming more common in the Southeast, largely due to expanding logging operations and the impact of wind/geohazard, especially hurricanes (Extended Data Fig. 5b (5)). By contrast, the size of anthropogenic disturbance patches associated with construction and agricultural disturbance is declining in many hexagonal grids (Extended Data Fig. 5b (2 and 3)). This potentially reflects trends towards intensification and more small-scale land use practices in those areas. However, their patch size is increasing in parts of the central USA due to new and large-scale developments. Wild disturbances (Extended Data Fig. 5b (4–6)), however, show a mixed pattern, with both increasing and decreasing patch sizes evident across different regions. The maximum patch size (per hexagonal grid and per year) of all three wild disturbance categories has generally expanded, reflecting the growing impact of extreme events (Extended Data Table 5). While most significant trends in patch size did not show clear acceleration or deceleration, a key pattern emerged. Decelerated trends, particularly those showing a decrease in patch size, were more prevalent than accelerated trends, suggesting a potential slowdown in both the expansion and contraction of disturbance patches across the USA.

The severity of land disturbance generally shows an upward trend (Fig. 4c), with 56% of hexagonal grids experiencing a significant increase (Extended Data Table 5). This increase is evident for most disturbance agents, suggesting a trend towards more intense disturbance events with potentially greater ecological consequences. However, a closer examination reveals that while severity is increasing, the pace of that increase is slowing down in many hexagonal grids and for most of the disturbance agents (Extended Data Fig. 5c (1–7)), indicating a potential future stabilization.

Discussion

Our results reveal the changing impact of human activities on US landscapes, making a shift from direct human disturbance towards indirect influence on overall disturbance regimes. Human-directed disturbances, such as logging, agricultural disturbance and construction, have dominated the past few decades, collectively accounting for nearly two thirds of the total disturbed area (Extended Data Table 3). However, we document a substantial decline in their frequency and extent, encompassing a wider range of land use modifications than previously documented[31,32]. For instance, the observed decline in agricultural disturbance probably reflects a combination of reduced expansion (as noted in earlier study[32]) and shifts away from certain agricultural practices, such as changes in irrigation, tillage or intensification patterns. Similarly, the decline in construction appears to reflect not only economic cycles but also potential shifts in development patterns.

This general decline in the USA contrasts with trends observed in other regions, such as rising forest harvest in Europe[33], rapid

https://doi.org/10.1038/s41561-025-01792-3

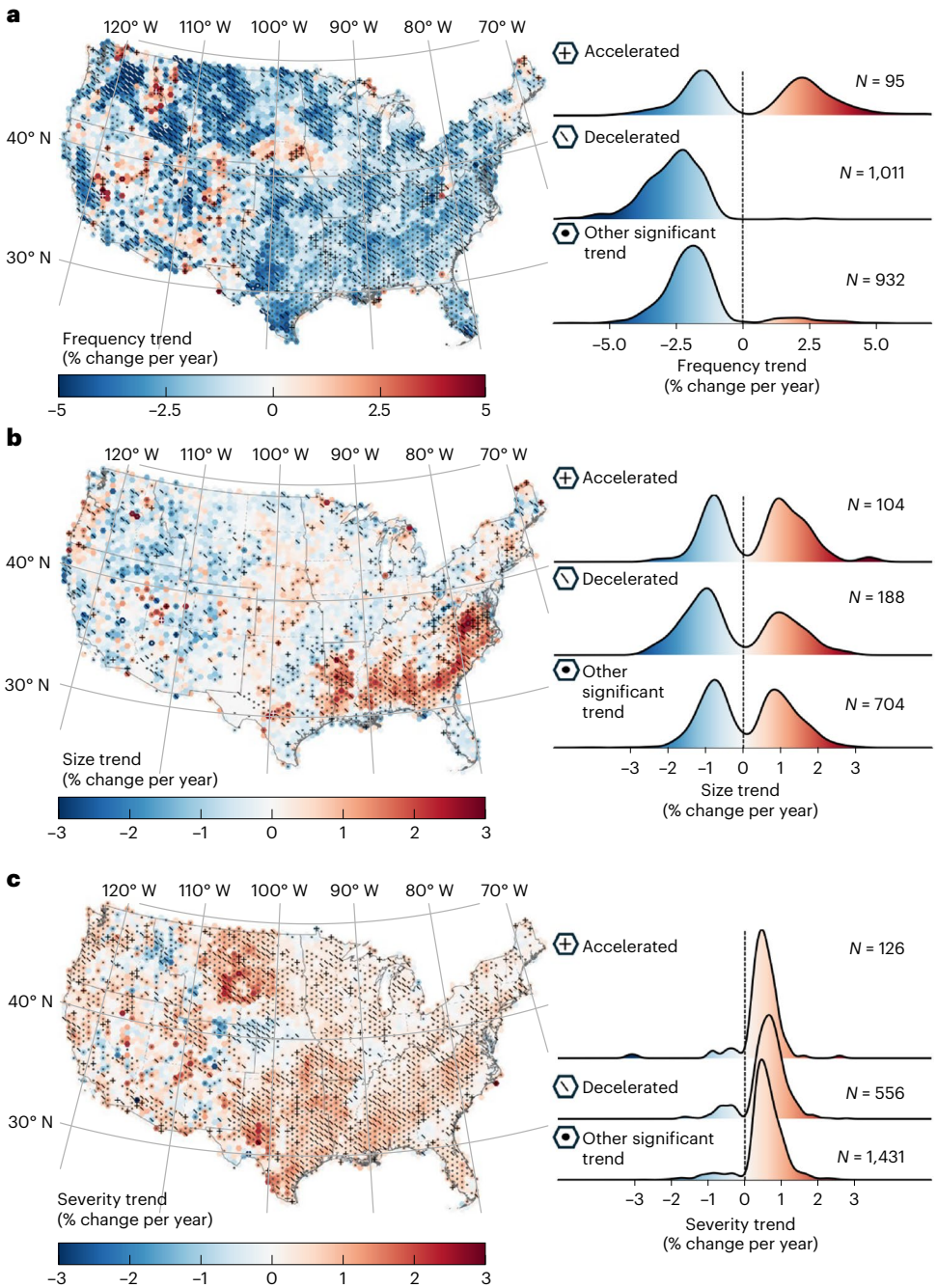

Fig. 4 | Land disturbance regime shifts across the USA in 2,500-km² hexagonal grids (1988–2022). a, Map of disturbance frequency trend. **b**, Map of disturbance size trend. **c**, Map of disturbance severity trend. Trends are estimated using the Theil–Sen estimator, and their statistical significance is determined by the two-tailed Mann–Kendall test ($P < 0.05$). Symbols indicate significantly accelerated (+) and decelerated (\) trends, while dots denote other significant (increasing or decreasing) trends. Each map features density plots based on landscapes with significant trends, illustrating the distribution of trend magnitudes in accelerated, decelerated and other significant trends. The number (*N*) represents the number of hexagonal grids with significant trend. All maps are shown in Albers equal-area conic projection. The solid boundaries represent US Fifth National Climate Assessment regions, while the dashed boundaries indicate state borders. The consistent colour scale across all maps facilitates direct comparison of disturbance regime shift patterns. Each individual disturbance agent regime trend for logging, construction, agricultural disturbance, stress, wind/geohazard, fire and water disturbance is provided in Extended Data Fig. 5.

urbanization in China[34], and agricultural expansion in Africa and South America[35]. These patterns probably reflect a combination of policy or practice changes (for example, sustainable forestry practices[36] and more emphasis on land conservation), technological advances in land management (for example, precision agriculture) and shifts in economic conditions in the USA, as well as outsourcing of resource extraction to other parts of the world. The USA, while still a major consumer of resources, has increasingly shifted the environmental burden of production to developing nations. This shift in resource production, while potentially contributing to reduced human-directed disturbances within the USA, raises important questions about the global distribution of environmental impacts and the equity of resource consumption.

This decline in direct human impact on the land does not signal a return to a pristine past. In some regions, such as the Northeast, where human impacts have been extensive for centuries, the decline

in disturbance we observe might simply reflect the fact that these landscapes have already been heavily modified, leaving less opportunity for new, large-scale disturbance. Yet, even as direct human land modification decreases, challenges emerge from indirect human influences that appear to be altering wild disturbance regimes. For instance, anthropogenic climate change could be one factor influencing the wild disturbances that reshape our ecosystems, potentially altering their frequency, size or severity through indirect mechanisms that are difficult to quantify directly. Rising global temperatures, a key manifestation of climate change, are associated with conditions potentially favouring more intense hurricanes, prolonged droughts and expanded ranges of forest pests, all of which can trigger or worsen wild force disturbances. Additionally, human activities are directly responsible for ignitions in many wildfires, whether through accidental or intentional means[37–39]. These indirect anthropogenic influences are challenging to quantify directly using satellite data, which primarily capture the proximate causes of disturbance[19]. Future research should prioritize integrating our remote sensing analysis with climate models, socioeconomic data and other sources, such as social media records of human-caused fires, to better disentangle the complex web of human influences.

This shift towards indirect human impacts is clearly reflected in the accelerating surge of wild forces across the USA. Our findings, based on a comprehensive, continental-scale analysis of 35 yr of Landsat data, provide a uniquely detailed view of this transformation. The western and central USA, regions already experiencing rising wildfire activity and widespread drought- and pest-induced stress, are experiencing the most marked increase in wild disturbances. While previous studies have documented the larger footprint and increased frequency of individual wild disturbances such as fire and stress[27,40,41], our analysis reveals a more comprehensive picture, highlighting several distinct patterns of accelerating or decelerating change across all wild agents and regime characteristics. For example, the frequency and patch size of wild disturbances are increasing at an accelerated rate across most regions, whereas their severity, while still increasing overall, is rising at a decelerated pace (Fig. 4). This suggests a potential shift towards more frequent, larger and potentially more impactful wild disturbance events in the future. These findings underscore the growing influence of wild disturbances on US landscapes, signalling a future of greater unpredictability.

Conclusion

The USA is entering a new era of disturbance. While our analysis suggests that human impacts are declining in some areas, this trend is accompanied by the accelerating surge of wild disturbances. Fire, stress and wind/geohazard are reshaping US ecosystems, driven by climate and other environmental changes, often amplified by past human actions. The escalating frequency, size and severity of these events pose profound challenges to landscape resilience and sustainability. We are moving from an era of relative human control to one where wild forces exert increasing influence, suggesting a more unpredictable and dynamic future. Traditional approaches to land management, focused on suppression and control, are proving increasingly ineffective[42]. Our high-resolution, multi-decadal dataset offers a critical lens to view this transformation, equipping scientists, policymakers and land managers with the knowledge to develop adaptive, resilience-based strategies. The challenge now is to transform our relationship with disturbance from one of control to one of coexistence.

Online content

Any methods, additional references, Nature Portfolio reporting summaries, source data, extended data, supplementary information, acknowledgements, peer review information; details of author contributions and competing interests; and statements of data and code availability are available at https://doi.org/10.1038/s41561-025-01792-3.

References

1. Pausas, J. G. & Leverkus, A. B. Disturbance ecology in human societies. *People Nat.* **5**, 1082–1093 (2023).
2. Thom, D. & Seidl, R. Natural disturbance impacts on ecosystem services and biodiversity in temperate and boreal forests. *Biol. Rev.* **91**, 760–781 (2016).
3. Ellis, E. C., Klein Goldewijk, K., Siebert, S., Lightman, D. & Ramankutty, N. Anthropogenic transformation of the biomes, 1700 to 2000. *Glob. Ecol. Biogeogr.* **19**, 589–606 (2010).
4. Foley, J. A. et al. Global consequences of land use. *Science* **309**, 570–574 (2005).
5. Seidl, R., Schelhaas, M. & Lexer, M. J. Unraveling the drivers of intensifying forest disturbance regimes in Europe. *Glob. Change Biol.* **17**, 2842–2852 (2011).
6. Rudel, T. K. et al. Agricultural intensification and changes in cultivated areas, 1970–2005. *Proc. Natl Acad. Sc. USA* **106**, 20675–20680 (2009).
7. Zeng, N. et al. Agricultural Green Revolution as a driver of increasing atmospheric CO_2 seasonal amplitude. *Nature* **515**, 394–397 (2014).
8. Rosenzweig, C. et al. Attributing physical and biological impacts to anthropogenic climate change. *Nature* **453**, 353–357 (2008).
9. Grinsted, A., Moore, J. C. & Jevrejeva, S. Projected Atlantic hurricane surge threat from rising temperatures. *Proc. Natl Acad. Sci. USA* **110**, 5369–5373 (2013).
10. Naumann, G. et al. Global changes in drought conditions under different levels of warming. *Geophys. Res. Lett.* **45**, 3285–3296 (2018).
11. Lehmann, P. et al. Complex responses of global insect pests to climate warming. *Front. Ecol. Environ.* **18**, 141–150 (2020).
12. Keane, R. in *Encyclopedia of Biodiversity* Vol. 2 (ed. Levin, S. A.) Ch. 389, 568–581 (Academic, 2013).
13. Turner, M. G. Disturbance and landscape dynamics in a changing world. *Ecology* **91**, 2833–2849 (2010).
14. Senf, C. & Seidl, R. Mapping the forest disturbance regimes of Europe. *Nat. Sustain.* **4**, 63–70 (2021).
15. Venter, O. et al. Sixteen years of change in the global terrestrial human footprint and implications for biodiversity conservation. *Nat. Commun.* **7**, 12558 (2016).
16. Nitze, I., Grosse, G., Jones, B. M., Romanovsky, V. E. & Boike, J. Remote sensing quantifies widespread abundance of permafrost region disturbances across the Arctic and Subarctic. *Nat. Commun.* **9**, 5423 (2018).
17. Kossin, J. P. Hurricane intensification along United States coast suppressed during active hurricane periods. *Nature* **541**, 390–393 (2017).
18. Bowman, D. M. J. S. et al. Vegetation fires in the Anthropocene. *Nat. Rev. Earth Environ.* **1**, 500–515 (2020).
19. Zhu, Z., Qiu, S. & Ye, S. Remote sensing of land change: a multifaceted perspective. *Remote Sens. Environ.* **282**, 113266 (2022).
20. Coops, N. C., Wulder, M. A. & Iwanicka, D. Large area monitoring with a MODIS-based disturbance index (DI) sensitive to annual and seasonal variations. *Remote Sens. Environ.* **113**, 1250–1261 (2009).
21. Hammer, D., Kraft, R. & Wheeler, D. Alerts of forest disturbance from MODIS imagery. *Int. J. Appl. Earth Obs. Geoinf.* **33**, 1–9 (2014).
22. Hansen, M. *OPERA Land Surface Disturbance Alert from Harmonized Landsat Sentinel-2 Product (Version 1)* (NASA EOSDIS Land Processes Distributed Active Archive Center, 2024); https://doi.org/10.5067/SNWG/OPERA_L3_DIST-ALERT-HLS_V1.001
23. Mildrexler, D. J., Zhao, M. & Running, S. W. Testing a MODIS global disturbance index across North America. *Remote Sens. Environ.* **113**, 2103–2117 (2009).

24. Zhu, Z. et al. Continuous monitoring of land disturbance based on Landsat time series. *Remote Sens. Environ.* **238**, 111116 (2020).
25. Oswalt, S. N., Smith, W. B., Miles, P. D. & Pugh, S. A. *Forest Resources of the United States, 2017: a Technical Document Supporting the Forest Service 2020 RPA Assessment* (U.S. Department of Agriculture, Forest Service, 2019); https://doi.org/10.2737/WO-GTR-97
26. Cannon, J. B., Peterson, C. J., Godfrey, C. M. & Whelan, A. W. Hurricane wind regimes for forests of North America. *Proc. Natl Acad. Sci. USA* **120**, e2309076120 (2023).
27. Iglesias, V., Balch, J. K. & Travis, W. R. U. S. Fires became larger, more frequent, and more widespread in the 2000s. *Sci. Adv.* **8**, eabc0020 (2022).
28. Russell, A. et al. A fire-use decision model to improve the United States' wildfire management and support climate change adaptation. *Cell Rep. Sustain.* **1**, 100125 (2024).
29. Rippey, B. R. The US drought of 2012. *Weather Clim. Extrem.* **10**, 57–64 (2015).
30. Marsooli, R., Lin, N., Emanuel, K. & Feng, K. Climate change exacerbates hurricane flood hazards along US Atlantic and Gulf Coasts in spatially varying patterns. *Nat. Commun.* **10**, 3785 (2019).
31. Auch, R. F. et al. Conterminous United States land-cover change (1985–2016): new insights from annual time series. *Land* **11**, 298 (2022).
32. Lark, T. J., Spawn, S. A., Bougie, M. & Gibbs, H. K. Cropland expansion in the United States produces marginal yields at high costs to wildlife. *Nat. Commun.* **11**, 4295 (2020).
33. Seidl, R. & Senf, C. Changes in planned and unplanned canopy openings are linked in Europe's forests. *Nat. Commun.* **15**, 4741 (2024).
34. Yang, X. J. China's rapid urbanization. *Science* **342**, 310 (2013).
35. Potapov, P. et al. Global maps of cropland extent and change show accelerated cropland expansion in the twenty-first century. *Nat. Food* **3**, 19–28 (2022).
36. Masek, J. G. et al. Recent rates of forest harvest and conversion in North America. *J. Geophys. Res. Biogeosci.* **116**, G00K03 (2011).
37. Syphard, A. D., Keeley, J. E., Pfaff, A. H. & Ferschweiler, K. Human presence diminishes the importance of climate in driving fire activity across the United States. *Proc. Natl Acad. Sci. USA* **114**, 13750–13755 (2017).
38. Harvey, B. J. Human-caused climate change is now a key driver of forest fire activity in the western United States. *Proc. Natl Acad. Sci. USA* **113**, 11649–11650 (2016).
39. Balch, J. K. et al. Human-started wildfires expand the fire niche across the United States. *Proc. Natl Acad. Sci. USA* **114**, 2946–2951 (2017).
40. Andreadis, K. M. & Lettenmaier, D. P. Trends in 20th century drought over the continental United States. *Geophys. Res. Lett.* **33**, L10403 (2006).
41. Creeden, E. P., Hicke, J. A. & Buotte, P. C. Climate, weather, and recent mountain pine beetle outbreaks in the western United States. *For. Ecol. Manag.* **312**, 239–251 (2014).
42. Kreider, M. R. et al. Fire suppression makes wildfires more severe and accentuates impacts of climate change and fuel accumulation. *Nat. Commun.* **15**, 2412 (2024).

Methods

We leveraged long-term historical Landsat data and advanced time series analysis algorithms to map detectable land disturbances and their associated agents across the USA from 1988 to 2022. The map production includes Landsat image compositing, training data collection, disturbance detection and agent classification. On the basis of a stratified random sample, we conducted accuracy assessment, unbiased area estimation and uncertainty quantification for the resulting product. Finally, we quantified land disturbance regimes and regime shifts in frequency, size and severity to provide a comprehensive understanding of land disturbance dynamics across the USA.

Data

Landsat data. We analyse 13.45 million Landsat images (cloud coverage ≤ 80%) from the Landsat Collection 2 Analysis Ready Data (ARD) archive, encompassing the period from 1982 to 2023 (Supplementary Fig. 1). Those images were provided in 5,000 × 5,000 30-m pixel tiles (150 km × 150 km), using the Albers equal-area conic projection. The archive included data from Landsat 4-5 Thematic Mapper, Landsat 7 Enhanced Thematic Mapper Plus and Landsat 8-9 Operational Land Imager/Thermal Infrared Sensor. The ARD provides consistently processed surface reflectance data, facilitating analysis across different sensors and time periods. We utilized the surface reflectance of several key spectral bands, including blue, green, red, near-infrared and two short-wave infrared (SWIR) bands. In addition to surface reflectance, we incorporated brightness temperature data from the thermal infrared band, which is sensitive to land surface temperature and can provide valuable information about disturbance events, such as fire. The quality assessment band, generated using the Function of mask (Fmask) algorithm[43], enabled masking of pixels affected by clouds, cloud shadows and snow/ice. To minimize the effects of bidirectional reflectance distribution function, we selected observations from a single orbit path with the smallest view zenith angles[19]. All Landsat data were composited into 32-day regular time series observations to eliminate the variation in temporal density of the observation data (Supplementary Fig. 2), using an adaptive compositing method[44] (Supplementary Methods 1).

Training data. Creating accurate land disturbance maps requires extensive and representative training data. We compiled a comprehensive training dataset by integrating multiple sources (for example, existing disturbance reference datasets, survey data, land cover maps and visual interpretation of high-resolution imagery), each providing unique insights into the diverse disturbance agents: Landscape Fire and Resource Management Planning Tools (LANDFIRE)[45] for logging, construction, stress and wind/geohazard; Land Cover Trends (LCT)[46] for logging, agricultural disturbance and construction; Monitoring Trends in Burn Severity (MTBS)[47] for fire; Insect and Disease Survey (IDS)[48] for stress-related disturbances; Global Surface Water (GSW)[49] for water disturbance; and the National Land Cover Database (NLCD)[50] for providing the land cover and land use background and disturbance training data sample refinement. To ensure high training data quality, we selected only disturbance patches detected by our algorithm (see the section entitled Land disturbance detection) that overlapped with the corresponding potential agent reference maps for over 50% of the pixels within each patch. When multiple agents were present in a simple disturbance patch, a majority rule was applied. Wind/geohazard samples were carefully interpreted using event reports (for example, hurricane, tornado and landslide) from the National Oceanic and Atmospheric Administration Severe Weather Database[51], the International Best Track Archive for Climate Stewardship[52] and the NASA (National Aeronautics and Space Administration) Global Landslide Catalog[53] to guarantee the training data quality. Details are documented in Supplementary Methods 2.

While LCLUC information from datasets such as LCT is valuable for identifying certain disturbance types (for example, conversion events such as deforestation, agriculture expansion or urbanization), this made up only part of our comprehensive training data. The NLCD provided essential land cover context for verifying samples (for example, ensuring construction occurred in non-forest areas, agricultural disturbance on farmland, stress within vegetation), but was not a direct source of disturbance training data. Our primary approach involved leveraging disturbance-specific datasets (for example, MTBS for fire, IDS for stress) substantially augmented by extensive visual interpretation. We visually analysed more than 60,000 sample patches, referencing preliminary disturbance maps, high-resolution Google Earth imagery and other relevant data (such as drought and pest maps), specifically to improve representation of agents less covered by existing datasets, including construction, stress and wind/geohazard. The spatial distribution of these combined training sample patches is shown in Supplementary Fig. 3.

Land disturbance detection. The foundation of our land disturbance mapping approach is the COntinuous monitoring of Land Disturbance (COLD) algorithm[24]. COLD, specifically designed for detecting disturbances from Landsat time series, offers several advantages over traditional change detection methods. First, it models the full Landsat time series, capturing both seasonal and interannual variability in surface reflectance. This allows for the detection of subtle disturbances that may be missed by methods that compare only two or a few images. Second, it provides information on the timing, magnitude and spectral characteristics of disturbances, providing valuable insights into the nature and potential drivers of these events.

COLD operates by fitting a harmonic time series model (equation (1)) to each Landsat pixel, using the least absolute shrinkage and selection operator[54] to select the most informative harmonic components (Supplementary Fig. 7). The model estimates expected spectral values for each observation date based on the historical time series. Stable pixels are those where observed values remain within the expected range of variability defined by the model. Disturbances are identified when six consecutive reflectance differences ($\Delta\rho$) between observations (ρ) and model predictions ($\hat{\rho}$) exceed a predefined threshold[24]. In this study, we used a threshold of 0.95 to slightly relax the detection criterion and reduce omission errors. This threshold indicates a statistically significant deviation from the established spectral pattern for that pixel. In COLD, only five Landsat spectral bands—green, red, near-infrared, SWIR1 and SWIR2—were used to detect disturbance, but all other bands were used for estimating their specific time series models that include rich temporal-spectral information. In this way, COLD can provide the disturbance location at the Landsat pixel, the disturbance time at the Landsat observation and the corresponding disturbance magnitude. The disturbance magnitude was calculated as the square root of the sum of the squared per-band change magnitude, which is calculated by the median differences (excluding the blue and thermal infrared bands) of the consecutive reflectance differences at the time of a detected break[24]. Disturbance magnitude is unitless, with a range of 0–1. To optimize computational efficiency, we reduced the model updating frequency from every new observation to every 4% of the number of observations used in previous model updating[24]. This can greatly (>60%) reduce the computation time and achieve similar detection accuracies. Although Landsat data from 1982 to 2023 were utilized (Supplementary Fig. 2), we focused on disturbance detection maps between 1988 and 2022. This is because data before 1988 were used to initialize time series models, and data after 2022 were used to confirm disturbances at the end of the time series. We excluded permanent water pixels from the GSW dataset[49] to focus exclusively on land-related disturbances.

$$\hat{\rho}_{i,t} = a_{0,i} + \sum_{k=1}^{3}\left\{a_{k,i}\cos\left(\frac{2\pi k}{T}t\right) + b_{k,i}\sin\left(\frac{2\pi k}{T}t\right)\right\} + c_{1,i}t \quad (1)$$

where t represents the Julian date, i represents the ith Landsat spectral band, k represents the temporal frequency of different harmonic components ($k = 1, 2$ and 3), T represents the average number of days per year ($T = 365.25$), $a_{0,i}$ is the coefficient for capturing the overall value for the ith Landsat spectral band, $a_{k,i}$ and $b_{k,i}$ are coefficients for capturing the intra-annual change for the ith Landsat spectral band, $c_{1,i}$ is the coefficient for capturing the interannual change for the ith Landsat spectral band, and $\hat{\rho}_{i,t}$ is the surface reflectance for the ith Landsat spectral band at Julian date t based on model prediction.

Land disturbance agent classification

To attribute the agent of land disturbance identified by COLD, in this study, we developed an object-based disturbance agent classification approach. Assuming that land disturbance events are spatially connected within a relatively short time (for example, one year), we segmented each disturbance object patch through eight-connected directions based on the COLD-detected annual per-pixel land disturbance maps. Objects with fewer than four pixels (about 0.4 ha) were filtered out, as this is usually the smallest unit that Landsat can reliably map[55]. Subsequently, we extracted samples from the existing training dataset to train random forest models, incorporating a total of 165 predictor variables from spectral, temporal and spatial domains. These models were then utilized to classify all pixels within each disturbance object patch, and a majority vote was applied to determine the disturbance patch's agent. We trained a separate random forest model for each Landsat ARD tile (Supplementary Fig. 3), using training data extracted from its surrounding 3 × 3 tiles.

Predictor variable. We gathered a total of 165 predictor variables for agent classification based on three categories: the COLD outputs, topographic information and object-based metrics of segmented disturbance patches (Supplementary Table 2). In terms of the first category, 121 predictor variables were derived from COLD, including parameters of pre-disturbance, during disturbance and after disturbance for each pixel and each event. For the disturbance event described by Supplementary Fig. 7, COLD created a time series model before disturbance (pre-disturbance model), created a time series model after disturbance (post-disturbance model) and generated during-disturbance information for each spectral band. The pre- and post-disturbance models indicate the land surface characteristics (based on model coefficients and root mean square error values described in equation (1)) before and after a disturbance, respectively. The during-disturbance information includes per-band change magnitude, as well as per-band change magnitude trend and variation. Most of the COLD output variables have been well documented by the literature[24], except for per-band change magnitude trend and variation. The per-band change magnitude trend represents the trend of the reflectance differences ($\Delta\rho$) between the model predictions and the observations during the change detection process (that is, six consecutive observations). A linear model based on ordinary least square regression is used to estimate the trend, and the change magnitude variation is calculated based on the corresponding root mean square error, which measures the regression uncertainty. We also used the change time to indicate when (day of year) a disturbance happened, and the change interval to describe how long the disturbance lasted (that is, period between the end of pre-disturbance model and the start of post-disturbance model), as this information could be helpful for disturbance agent attribution.

For the topographic predictor variables, we included elevation, slope and aspect, all of which have shown promise in classifying disturbance agents[56–58]. We also computed the spatial metrics for each disturbance object because different disturbance agents usually have varied spatial patterns. First, we computed the disturbance object textures represented by the standard deviations of change time, change magnitude and change interval from all pixels within the same disturbance object. Then, we calculated 12 spatial predictor variables to describe the spatial characteristics of the disturbance object, such as size, form and shape, using FRAGSTATS—a spatial pattern analysis program for quantifying landscape structure[59]. In addition, we computed the elevation range for each disturbance object as one of the predictor variables as this could also relate to the type of disturbance agent. For example, a geohazard caused by landslide would be more likely to occur in regions with large elevation differences.

Classification model and strategy. We used a random forest model[60] with 100 decision trees to balance computational efficiency and classification accuracy. The training data of the random forest are pixel-based, instead of at the object-level, as this can provide many more training sample units with large variations of spectral information. For training pixels within the same disturbance patch, they will share the same values in the patch-based variables (Supplementary Table 2). Ideally, the number of training sample units for each class is based on its area proportion with some limits on dominant and rare classes[61]. However, there is no way to know the area proportion for each class before we have a map of them. To solve this chicken-and-egg dilemma, we used an iterative procedure to optimize training data selection (Supplementary Methods 3). First, we created a preliminary disturbance agent classification map using an equal distribution of pixel-based training data. Then, using the class proportions derived from this preliminary map (with a minimum of 3% and a maximum of 40% per class)[61], we extracted a proportionally distributed dataset to train a new random forest model which was used to generate the final land disturbance agent map. This proportional sampling strategy, evaluated using five diverse regions across the USA (Supplementary Fig. 4), outperformed equal sampling and achieved a stable accuracy using 10,000 training pixels (Supplementary Fig. 5).

Refining classification map. We conducted a rigorous manual refinement process to refine the initial USA-wide disturbance agent maps derived from open-source training data. We identified areas of classification error in the preliminary maps, such as confusion between construction and agricultural disturbance, stress (for example, drought) and climate variability, water disturbance and agricultural disturbance (for example, irrigation), and wind/geohazard and logging. At these locations, we visually interpreted high-resolution imagery and added over 60,000 manually refined training samples to update the random forest models (Supplementary Fig. 3). This iterative refinement process was essential for achieving high classification accuracy and ensuring the reliability of our final disturbance agent maps. These refined samples were also incorporated into the training of final USA-wide maps in cases where the pre-train models were having issues.

Accuracy assessment and unbiased area estimation

We used the three most widely used metrics, including overall accuracy, user's accuracy and producer's accuracy, and followed the 'good practice' recommendation[62]. We used an unbiased estimator of area based on the reference sample data and used the map to improve precision of the area estimates. We selected a set of stratified random validation samples using land disturbance agent types as the strata. In this stratification, each sample plot represents a location on the ground (30 m) and a time (calendar year). We selected 907 sample plots across strata, as detailed in Extended Data Table 2, to achieve a target standard error of 0.01 for overall accuracy and an expected user's accuracy of 0.7. This set of validation data was used to evaluate the accuracy of both the disturbance time and disturbance agent. We interpreted all of the validation sample plots using Landsat time series, high-resolution images from Google Earth, Planet Scope images, hurricane/tornado records, and other auxiliary data such as drought index and insect survey data. Disturbance detection and agent classification results were masked during interpretation to

ensure independence. Agreement was defined as a match in both disturbance status (disturbed or not) and agent category between the reference data and our map within the same calendar year. Stratified estimators of accuracy and area along with their accompanying standard errors were produced using an indicator variable formulation[63]. We acknowledge that, while increasing the validation sample size can reduce uncertainty in the accuracy assessment and unbiased area estimation, our current sample size is sufficient to capture the dominant patterns at the national scale, in accordance with the statistical 'good practice' recommendation[62]. The rare disturbance classes (for example, wind/geohazard), which tend to have higher uncertainty, represent only a small fraction of the total area—particularly within subregions (Extended Data Table 3)—and do not affect our overall scientific conclusions.

Disturbance regime metrics

We analysed disturbance regimes across the USA by quantifying their characteristics at a landscape scale, using a grid of 3,391 hexagonal grids (2,500 km^2 or 0.25 Mha) to ensure consistent spatial analysis. Each disturbance patch was generated through eight-connected directions based on each annual disturbance agent map (35-yr disturbance agent maps total). We then calculated three key regime metrics for each disturbance agent within each grid, following the methodology of ref. 14, in which we calculated disturbance frequency (units of patches per square kilometre per year), disturbance size (units of hectare) and disturbance severity (unitless). Disturbance frequency reflects the rate of disturbance occurrence within a landscape, measured as the number of individual disturbance patches per square kilometre per year. Disturbance size quantifies the area of each individual patch, which is calculated by the number of disturbed pixels multiplied by pixel size (0.09 ha). Disturbance severity measures the impact of each individual disturbance patch based on its disturbance magnitude in Landsat spectral bands derived from our detection algorithm[24]. We normalized severity using quartile percentiles of the mean disturbance magnitude (average of all pixel-level disturbance magnitudes within the same patch) for each disturbance agent spanning 35 yr and USA-wide to enable comparisons across different disturbance agents. This resulted in a continuous severity scale ranging from 1 (low) to 4 (very high), reflecting the severity of the disturbance (Extended Data Table 4). Finally, to visualize and analyse the regime indicators, we aggregate the frequency, size and severity of disturbance patches at the landscape level (hexagonal grid) using the arithmetic mean for patches intersecting each grid from 1988 to 2022.

Quantifying disturbance regime shifts

We quantified the temporal trends in both total disturbance footprint (nationally) and individual disturbance regime metrics (at the landscape scale) in the past 35 yr. We used the non-parametric Theil–Sen regression, which is robust to outliers, to estimate linear trends, with significance assessed ($P < 0.05$) via the two-tailed Mann–Kendall test[64]. Recognizing that disturbance regimes often exhibit nonlinear dynamics, we performed a second-level trend analysis using a 10-yr rolling window. For each window (from 1997 to 2022), we estimated the trend in each regime metric (frequency, size or severity). We then applied Theil–Sen regression to these slopes to identify whether the trends themselves were accelerating or decelerating over time, and with significance assessed ($P < 0.05$) via the Man–Kendall test. An accelerating trend was defined as a positive trend becoming more positive (or a negative trend becoming more negative), while a decelerating trend indicated a positive trend becoming less positive (or a negative trend becoming less negative). This two-level approach allowed us not only to capture temporal shifts in disturbance regimes but also to identify periods of accelerating or decelerating changes.

Data availability

The open-source data include regions of the Fifth National Climate Assessment at https://toolkit.climate.gov/NCA5, USGS Landsat Collection 2 US ARD at https://earthexplorer.usgs.gov, 2012 State Boundaries of United States and Territories at https://purl.stanford.edu/vt021tk4894, Public Events Geodatabase 1999–2022 (Model Ready Events) of LANDFIRE at https://landfire.gov, LCT by https://www.usgs.gov/centers/western-geographic-science-center/science/land-cover-trends, Fire Occurrence Dataset 1984–2022 of MTBS at https://www.mtbs.gov, NLCD 2001–2021 at https://www.usgs.gov/centers/eros/science/national-land-cover-database, Yearly Seasonality of GSW version 1.4 at https://global-surface-water.appspot.com, IDS at https://www.fs.usda.gov/science-technology/data-tools-products/fhp-mapping-reporting/detection-surveys, Severe Weather Database at https://www.spc.noaa.gov, International Best Track Archive for Climate Stewardship at https://www.ncei.noaa.gov/products/international-best-track-archive, Global Landslide Catalog at https://gpm.nasa.gov/landslides/projects.html#GLC and Shuttle Radar Topography Mission (GL1) 30m DEM version 3 at https://lpdaac.usgs.gov/products/srtmgl1v003. The 1988–2022 disturbance dataset generated by this study is available via GitHub at https://github.com/gersl/usdist.

Code availability

The disturbance dataset and analyses were produced with custom code using MATLAB 2022b and Python 3.10 (available via GitHub at https://github.com/gersl/usdist).

References

43. Zhu, Z., Wang, S. & Woodcock, C. E. Improvement and expansion of the Fmask algorithm: cloud, cloud shadow, and snow detection for Landsats 4-7, 8, and Sentinel 2 images. *Remote Sens. Environ.* **159**, 269–277 (2015).
44. Qiu, S., Zhu, Z., Olofsson, P., Woodcock, C. E. & Jin, S. Evaluation of Landsat image compositing algorithms. *Remote Sens. Environ.* **285**, 113375 (2023).
45. Rollins, M. G. LANDFIRE: a nationally consistent vegetation, wildland fire, and fuel assessment. *Int. J. Wildland Fire* **18**, 235–249 (2009).
46. Loveland, T. R. et al. A strategy for estimating the rates of recent United States land-cover changes. *Photogramm. Eng. Remote Sens.* **68**, 1091–1099 (2002).
47. Sparks, A. M. et al. An accuracy assessment of the MTBS burned area product for shrub-steppe fires in the northern Great Basin, United States. *Int. J. Wildland Fire* **24**, 70–78 (2015).
48. Johnson, E. W. & Wittwer, D. Aerial detection surveys in the United States. In *2006 Monitoring Science and Technology Symposium: Unifying Knowledge for Sustainability in the Western Hemisphere Proceedings RMRS-P-42CD* (eds Aguirre-Bravo, C. et al.) 809–811 (U.S. Department of Agriculture, Forest Service, Rocky Mountain Research Station, 2008).
49. Pekel, J. F., Cottam, A., Gorelick, N. & Belward, A. S. High-resolution mapping of global surface water and its long-term changes. *Nature* **540**, 418–422 (2016).
50. Jin, S. et al. Overall methodology design for the United States National Land Cover Database 2016 products. *Remote Sens.* **11**, 2971 (2019).
51. *Severe Weather Data Inventory* (NOAA). https://www.ncei.noaa.gov/products/severe-weather-data-inventory. Accessed 1 Sept 2025.
52. Knapp, K. R., Kruk, M. C., Levinson, D. H., Diamond, H. J. & Neumann, C. J. The International Best Track Archive for Climate Stewardship (IBTrACS): unifying tropical cyclone data. *Bull. Am. Meteorol. Soc.* **91**, 363–376 (2010).
53. Kirschbaum, D. B., Adler, R., Hong, Y., Hill, S. & Lerner-Lam, A. A global landslide catalog for hazard applications: method, results, and limitations. *Nat. Hazards* **52**, 561–575 (2010).

54. Tibshirani, R. Regression shrinkage and selection via the lasso. *J. R. Stat. Soc. B* **58**, 267–288 (1996).
55. Dobson, J. E. *NOAA Coastal Change Analysis Program (C-CAP): Guidance for Regional Implementation* (NOAA, 1995); https://coast.noaa.gov/data/digitalcoast/pdf/ccap-regional-guidance.pdf
56. Kennedy, R. E. et al. Attribution of disturbance change agent from Landsat time-series in support of habitat monitoring in the Puget Sound region, USA. *Remote Sens. Environ.* **166**, 271–285 (2015).
57. Sebald, J., Senf, C. & Seidl, R. Human or natural? Landscape context improves the attribution of forest disturbances mapped from Landsat in Central Europe. *Remote Sens. Environ.* **262**, 112502 (2021).
58. Zhang, Y. et al. Mapping causal agents of disturbance in boreal and arctic ecosystems of North America using time series of Landsat data. *Remote Sens. Environ.* **272**, 112935 (2022).
59. McGarigal, K. & Marks, B. J. *FRAGSTATS: Spatial Pattern Analysis Program for Quantifying Landscape Structure* PNW-GTR-351 (U.S. Department of Agriculture, Forest Service, Pacific Northwest Research Station, 1995); https://doi.org/10.2737/PNW-GTR-351
60. Breiman, L. Random forests. *Mach. Learn.* **45**, 5–32 (2001).
61. Zhu, Z. et al. Optimizing selection of training and auxiliary data for operational land cover classification for the LCMAP initiative. *ISPRS J. Photogramm. Remote Sens.* **122**, 206–221 (2016).
62. Olofsson, P. et al. Good practices for estimating area and assessing accuracy of land change. *Remote Sens. Environ.* **148**, 42–57 (2014).
63. Stehman, S. V. Estimating area and map accuracy for stratified random sampling when the strata are different from the map classes. *Int. J. Remote Sens.* **35**, 4923–4939 (2014).
64. Wilcox, R. R. *Fundamentals of Modern Statistical Methods: Substantially Improving Power and Accuracy* (Springer, 2010).

Acknowledgements

Z.Z. and S.Q. acknowledge support from United States Geological Survey–NASA 2018–2023 Landsat Science Team contract number 140G0119C0008 (Toward Near Real-time Monitoring and Characterization of Land Surface Change for the Conterminous US). The computational work for this project was conducted using resources provided by the Storrs High-Performance Computing cluster. We thank the University of Connecticut Storrs High-Performance Computing facility and its team for their resources and support, which aided in achieving these results. Any use of trade, firm or product names is for descriptive purposes alone and does not imply endorsement by the US Government. We acknowledge the use of an AI-based language tool to improve the clarity and readability of the paper, and all content was reviewed and approved by the authors.

Author contributions

Conceptualization: S.Q., Z.Z. and C.E.W.; methodology: S.Q., Z.Z. and X.Y.; production: S.Q.; validation: S.Q., Z.Z., X.Y., M.C., A.G., F.H., K.S., J.W.S., T.L. and S.S.; formal analysis: S.Q. and Z.Z.; resources: Z.Z.; writing (original draft): S.Q. and Z.Z.; writing (review and editing): S.Q., Z.Z., X.Y., C.E.W., R.T.F., S.S., Y.Z., M.C., A.G., F.H., K.S., J.W.S., T.L., W.R. and R.R.N.; funding acquisition: Z.Z.

Competing interests

The authors declare no competing interests.

Additional information

Extended data is available for this paper at https://doi.org/10.1038/s41561-025-01792-3.

Supplementary information The online version contains supplementary material available at https://doi.org/10.1038/s41561-025-01792-3.

Correspondence and requests for materials should be addressed to Shi Qiu or Zhe Zhu.

Peer review information *Nature Geoscience* thanks Martin Herold and the other, anonymous, reviewer(s) for their contribution to the peer review of this work. Primary Handling Editors: Camilla Brunello and Xujia Jiang, in collaboration with the *Nature Geoscience* team.

https://doi.org/10.1038/s41561-025-01792-3

Extended Data Table 1 | Definition of the land disturbance causal agent classes

Classifications		Description
Human-directed	**Logging**	Human-induced removal of trees from a forested area.
	Construction	Lands (either in a vegetated or non-vegetated state) cleared for development (for example, buildings, mining, solar panels, and golf course) or previously built-up land (also including concrete parking lot) is intensified with new structures.
	Agricultural disturbance	Lands, where agriculture activities are the major cause of the disturbance, such as agriculture expansion, intensification, and abandonment, as well as changes in management practices (for example, changing irrigation methods, shifting to different crops, with/without cover crops, rotation change, and tillage practice changes).
Wild	**Stress**	Vegetated lands, where the condition of vegetations (that is, grass, shrub, and tree) is changed to a less favorable status by natural factors, such as exotic pests or pathogen outbreaks, and drought.
	Wind/ geohazard	Lands scattered with natural or artificial materials were physically damaged by wind (for example, hurricanes, tornadoes, storms) and geohazard (for example, landslides, earthquakes, volcanic eruptions, and tsunamis).
	Fire	Burned areas due to wildfires or prescribed fires on all land surfaces, such as forests, shrublands, or grasslands.
Water disturbance		A rising and overflowing of water onto normally dry land (for example, flooding), or the decrease of water resulting in the conversion of formerly waterlogged areas into dry land. It can occur during heavy rains, when ocean waves come on shore, when snow melts quickly, when dams or levees break, or when water diversion structures were changed.
Other	Natural vegetation succession	The land cover types are altered by the process of the structure of a biological community changing over time (for example, transitioned from grass to shrub, and all the way to forest) with enough time and adequate recovery speed.
	Climate variability	The short-term variations in climate patterns (for example, months, seasons, or years).
	Variation in water quality	Variations in the chemical composition, physical characteristics, biological parameters, pH levels, temperature fluctuations, and source contamination of water.
	False-positive change	False-positive change signals induced by clouds, shadows, and change detection algorithms.
	Isolated disturbance	Any disturbance less than minimum mapping unit, that is, four Landsat pixels.
	Stable	The absence of changes in land cover types and a lack of variations in spectral bands of satellite remote sensing data over time.

The first disturbance over time was identified if multiple disturbances occurred within one year, and only the disturbance that has caused lasting (>6 months) ecological impacts will be mapped. This study primarily focuses on mapping and analyzing the seven land disturbance causal agent classes listed in the table, with the exception of the "other" category.

https://doi.org/10.1038/s41561-025-01792-3

Extended Data Table 2 | Confusion matrices and accuracy estimates for land disturbance agent map (1988-2022)

	Logging	Construction	Agricultural disturbance	Stress	Wind/ geohazard	Fire	Water disturbance	Other
Confusion matrix of sample counts (Unit: pixel)								
Logging	78	0	0	2	2	0	0	18
Construction	1	85	5	0	0	0	2	7
Agricultural disturbance	1	2	67	3	0	0	4	23
Stress	1	0	2	95	0	0	0	2
Wind/geohazard	22	3	4	0	56	2	4	9
Fire	0	0	0	3	0	85	3	9
Water disturbance	0	0	2	1	0	0	90	7
Other	0	0	0	0	0	0	0	207
Confusion matrix of area proportions (Unit: %)								
Logging	0.2108	0.0000	0.0000	0.0054	0.0054	0.0000	0.0000	0.0486
Construction	0.0005	0.0456	0.0027	0.0000	0.0000	0.0000	0.0011	0.0038
Agricultural disturbance	0.0023	0.0045	0.1519	0.0068	0.0000	0.0000	0.0091	0.0521
Stress	0.0008	0.0000	0.0016	0.0746	0.0000	0.0000	0.0000	0.0016
Wind/geohazard	0.0016	0.0002	0.0003	0.0000	0.0042	0.0001	0.0003	0.0007
Fire	0.0000	0.0000	0.0000	0.0020	0.0000	0.0564	0.0020	0.0060
Water disturbance	0.0000	0.0000	0.0014	0.0007	0.0000	0.0000	0.0629	0.0049
Other	0.0000	0.0000	0.0000	0.0000	0.0000	0.0000	0.0000	99.2272
Accuracy estimates								
User's accuracy (%)	78.00±8.16	85.00±7.03	67.00±9.26	95.00±4.29	56.00±9.78	85.00±7.03	90.00±5.91	100.00±0.00
Producer's accuracy (%)	97.58±2.21	90.56±11.27	96.23±2.33	83.36±10.24	43.44±34.35	99.74±0.36	83.51±10.18	99.88±0.03

The overall accuracy is 99.83±0.03. The columns represent the reference classification, and the rows represent the map classification (strata). The uncertainty ± indicates the margin of error of a 95% confidence interval. The validation sample size was determined for the purpose of evaluating US-wide maps, following the mathematical guidelines outlined in the "good practice" recommendation[62].

https://doi.org/10.1038/s41561-025-01792-3

Extended Data Table 3 | Total disturbance area 1988-2022 at national and Fifth National Climate Assessment regions

Region	Sample size	Total disturbance area 1988-2022 of different types (Mha)							
		Land disturbance	Human-directed			Wild			Water disturbance
			Logging	Construction	Agricultural disturbance	Stress	Wind/ geohazard	Fire	
US	907	178.50±7.74	58.85±6.15	13.73±1.99	43.00±5.81	24.38±3.13	2.60±2.04	15.40±1.27	20.54±2.74
Northeast	29	3.56±3.35	2.36±2.94	0.90±0.72	*ne*	*ne*	*ne*	*ne*	0.30±0.44
Midwest	64	7.23±4.01	1.55±1.79	1.62±0.92	2.44±2.39	0.58±1.16	*ne*	*ne*	1.04±0.95
Southeast	266	62.49±21.32	43.73±15.38	5.45±2.36	3.49±4.14	*ne*	1.84±1.60	0.75±0.66	7.23±4.03
Northern great plains	110	17.21±6.86	1.41±2.78	0.14±0.28	6.16±3.75	4.00±2.32	*ne*	1.99±1.35	3.52±1.67
Southern great plains	152	36.75±14.53	5.65±4.30	3.72±2.44	13.04±6.79	10.38±4.64	0.03±0.05	0.84±0.98	3.11±1.79
Northwest	72	13.27±7.09	4.33±3.61	*ne*	4.38±2.93	*ne*	0.62±1.24	3.10±1.92	0.85±0.82
Southwest	214	37.31±11.91	0.68±1.34	1.65±0.96	12.27±5.95	8.79±3.23	0.00±0.00	8.60±2.86	5.30±2.93

The areas were estimated according to the validation sample in Extended Data Table 2 and the indicator variable formulation of the estimators [63]. The uncertainty ± indicates the margin of error of a 95% confidence interval. ne means "not estimated" area due to insufficient sample size (N ≤ 1) in the subregions, reflecting a rare proportion of less than 1%.

https://doi.org/10.1038/s41561-025-01792-3

Extended Data Table 4 | Distribution of the frequency, size and severity of land disturbances across the US (1988-2022)

Regime indicator	Disturbance	Mean	Quantiles (%)				
			1	25	50	75	99
Landscape frequency (patches per km^2 per year)	Land disturbance	0.36	0.00	0.11	0.24	0.49	1.63
	Logging	0.09	0.00	0.00	0.01	0.09	0.71
	Construction	0.05	0.00	0.00	0.01	0.05	0.59
	Agricultural disturbance	0.13	0.00	0.01	0.05	0.15	1.07
	Stress	0.01	0.00	0.00	0.00	0.00	0.12
	Wind/geohazard	0.004	0.00	0.00	0.00	0.00	0.08
	Fire	0.01	0.00	0.00	0.00	0.00	0.09
	Water disturbance	0.07	0.00	0.01	0.02	0.05	1.08
Patch size (ha)	Land disturbance	2.51	0.18	0.45	0.63	1.26	25.56
	Logging	3.06	0.36	0.45	0.72	1.80	41.58
	Construction	1.24	0.36	0.36	0.54	1.08	11.07
	Agricultural disturbance	1.64	0.36	0.45	0.63	1.17	18.09
	Stress	16.82	0.36	0.36	0.54	0.90	15.75
	Wind/geohazard	2.42	0.36	0.45	0.63	1.08	22.86
	Fire	10.72	0.36	0.45	0.81	2.07	110.52
	Water disturbance	1.47	0.09	0.36	0.54	0.99	13.68
Patch magnitude (unitless; 0-1)	Land disturbance	0.16	0.05	0.11	0.15	0.20	0.38
	Logging	0.12	0.05	0.09	0.11	0.14	0.25
	Construction	0.17	0.07	0.12	0.16	0.20	0.40
	Agricultural disturbance	0.19	0.08	0.14	0.18	0.23	0.37
	Stress	0.09	0.04	0.06	0.08	0.11	0.21
	Wind/geohazard	0.11	0.05	0.08	0.10	0.13	0.25
	Fire	0.10	0.05	0.08	0.10	0.12	0.20
	Water disturbance	0.19	0.06	0.13	0.17	0.23	0.50
Patch severity (unitless; 1-4)	Land disturbance	2.51	1.00	2.00	3.00	3.00	4.00
	Logging	2.51	1.00	1.00	3.00	4.00	4.00
	Construction	2.50	1.00	2.00	2.00	4.00	4.00
	Agricultural disturbance	2.53	1.00	2.00	3.00	3.00	4.00
	Stress	2.57	1.00	2.00	3.00	4.00	4.00
	Wind/geohazard	2.49	1.00	2.00	3.00	3.00	4.00
	Fire	2.45	1.00	2.00	2.00	3.00	4.00
	Water disturbance	2.49	1.00	1.00	3.00	3.00	4.00

The landscape was represented by 2500-km^2 hexagonal grid.

https://doi.org/10.1038/s41561-025-01792-3

Extended Data Table 5 | Distribution of landscape-level regime trends across the US (1988-2022)

Regime	Disturbance	Trend				Changing rate of trend					
		Percent of trends		Percent of significant trends		Percent of significantly positive trends			Percent of significantly negative trends		
		Positive	Negative	Positive	Negative	Accelerated	Decelerated	Other	Accelerated	Decelerated	Other
Landscape frequency	Land disturbance	15%	83%	4%	56%	38%	5%	58%	2%	53%	45%
	Logging	30%	35%	15%	20%	31%	4%	65%	12%	18%	70%
	Construction	12%	65%	5%	46%	16%	10%	75%	3%	32%	65%
	Agricultural disturbance	4%	83%	1%	69%	43%	13%	43%	0%	75%	24%
	Stress	19%	11%	11%	6%	25%	5%	70%	3%	32%	65%
	Wind/geohazard	11%	3%	10%	2%	27%	4%	69%	0%	47%	53%
	Fire	12%	4%	7%	1%	32%	2%	66%	4%	14%	82%
	Water disturbance	34%	52%	9%	21%	20%	7%	73%	3%	41%	56%
Mean patch size	Land disturbance	43%	56%	15%	15%	12%	15%	73%	9%	22%	69%
	Logging	36%	32%	17%	12%	22%	7%	71%	5%	27%	68%
	Construction	29%	54%	8%	18%	8%	8%	84%	9%	17%	73%
	Agricultural disturbance	24%	65%	3%	24%	27%	6%	67%	5%	25%	70%
	Stress	15%	16%	6%	5%	10%	11%	79%	4%	23%	73%
	Wind/geohazard	9%	5%	7%	2%	8%	22%	70%	2%	18%	80%
	Fire	8%	9%	3%	2%	15%	7%	78%	2%	30%	68%
	Water disturbance	27%	66%	2%	16%	17%	9%	74%	6%	21%	73%
Maximum patch size	Land disturbance	31%	67%	4%	19%	25%	4%	71%	4%	36%	60%
	Logging	33%	34%	11%	10%	28%	2%	70%	5%	29%	66%
	Construction	20%	61%	3%	26%	23%	3%	74%	3%	26%	71%
	Agricultural disturbance	12%	77%	2%	42%	17%	6%	77%	2%	47%	51%
	Stress	17%	14%	8%	6%	20%	2%	78%	3%	27%	70%
	Wind/geohazard	10%	4%	7%	2%	22%	4%	74%	3%	35%	62%
	Fire	10%	7%	5%	2%	28%	2%	70%	2%	18%	80%
	Water disturbance	27%	62%	3%	15%	19%	6%	75%	2%	33%	65%
Mean patch severity	Land disturbance	79%	19%	56%	6%	6%	26%	68%	6%	32%	63%
	Logging	50%	14%	33%	4%	3%	27%	70%	11%	20%	70%
	Construction	73%	5%	60%	1%	5%	25%	71%	14%	4%	82%
	Agricultural disturbance	62%	24%	37%	8%	8%	24%	69%	8%	26%	65%
	Stress	17%	7%	9%	2%	7%	13%	80%	10%	9%	81%
	Wind/geohazard	11%	2%	8%	1%	2%	29%	69%	10%	0%	90%
	Fire	11%	4%	4%	1%	9%	11%	81%	5%	25%	70%
	Water disturbance	74%	14%	42%	2%	6%	18%	76%	13%	10%	77%

The landscape was represented by 2500-km^2 hexagonal grid.

https://doi.org/10.1038/s41561-025-01792-3

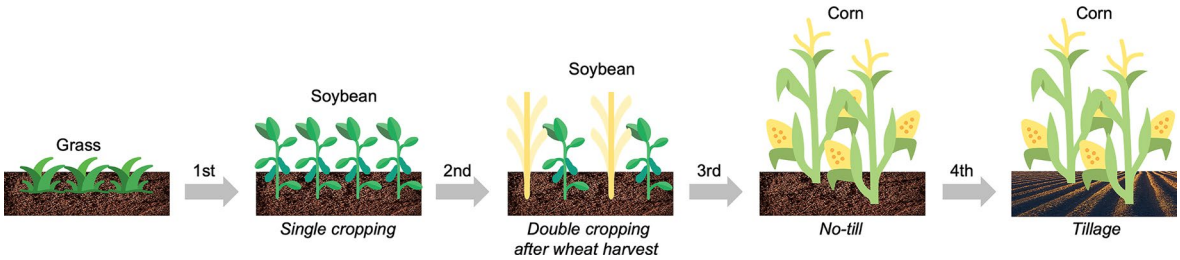

Extended Data Fig. 1 | Illustration of agricultural disturbance vs cropland expansion. This place experienced four disturbances in total, including one time crop expansion during the study period. The first disturbance is cropland expansion-1st (land conversion from grassland to cropland). The following three agricultural disturbances include agricultural intensification-2nd from single cropping to double cropping of soybeans, crop type change-3rd from soybean to corn, and agricultural practice change-4th from no-till to tillage. Plant icons adapted from Flaticon.com.

https://doi.org/10.1038/s41561-025-01792-3

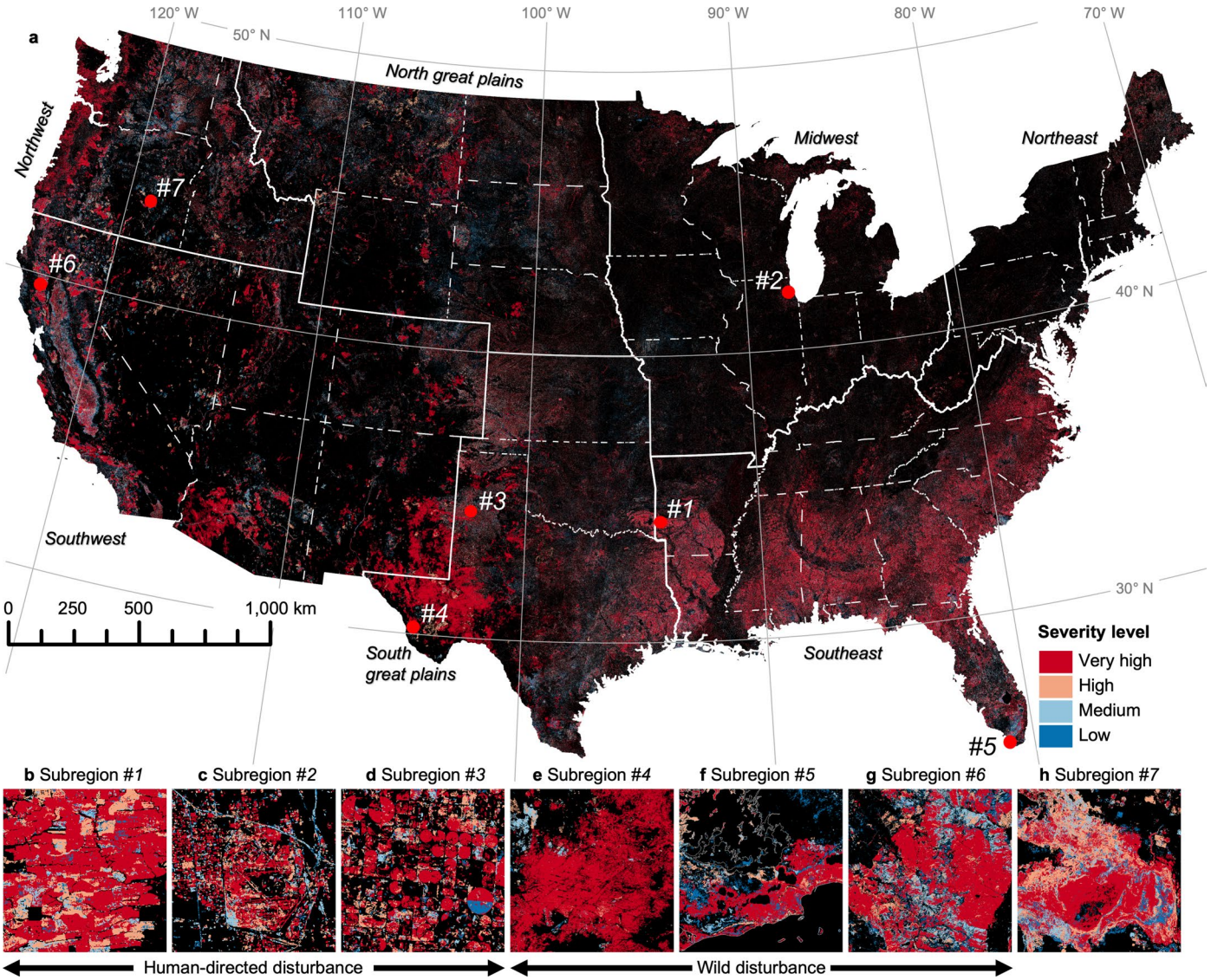

Extended Data Fig. 2 | Land disturbance severity maps across the US (1988-2022). a. US-wide map highlighting each pixel's most recent disturbances severity. The solid boundaries represent US Fifth National Climate Assessment regions, while the dashed boundaries indicate state border. **b-h.** Examples of disturbance agents from locations #1-7 of the US include logging, construction, agricultural disturbance, stress, wind/geohazard, fire, and water disturbance, respectively. The corresponding disturbance agent maps are presented in Fig. 1.

https://doi.org/10.1038/s41561-025-01792-3

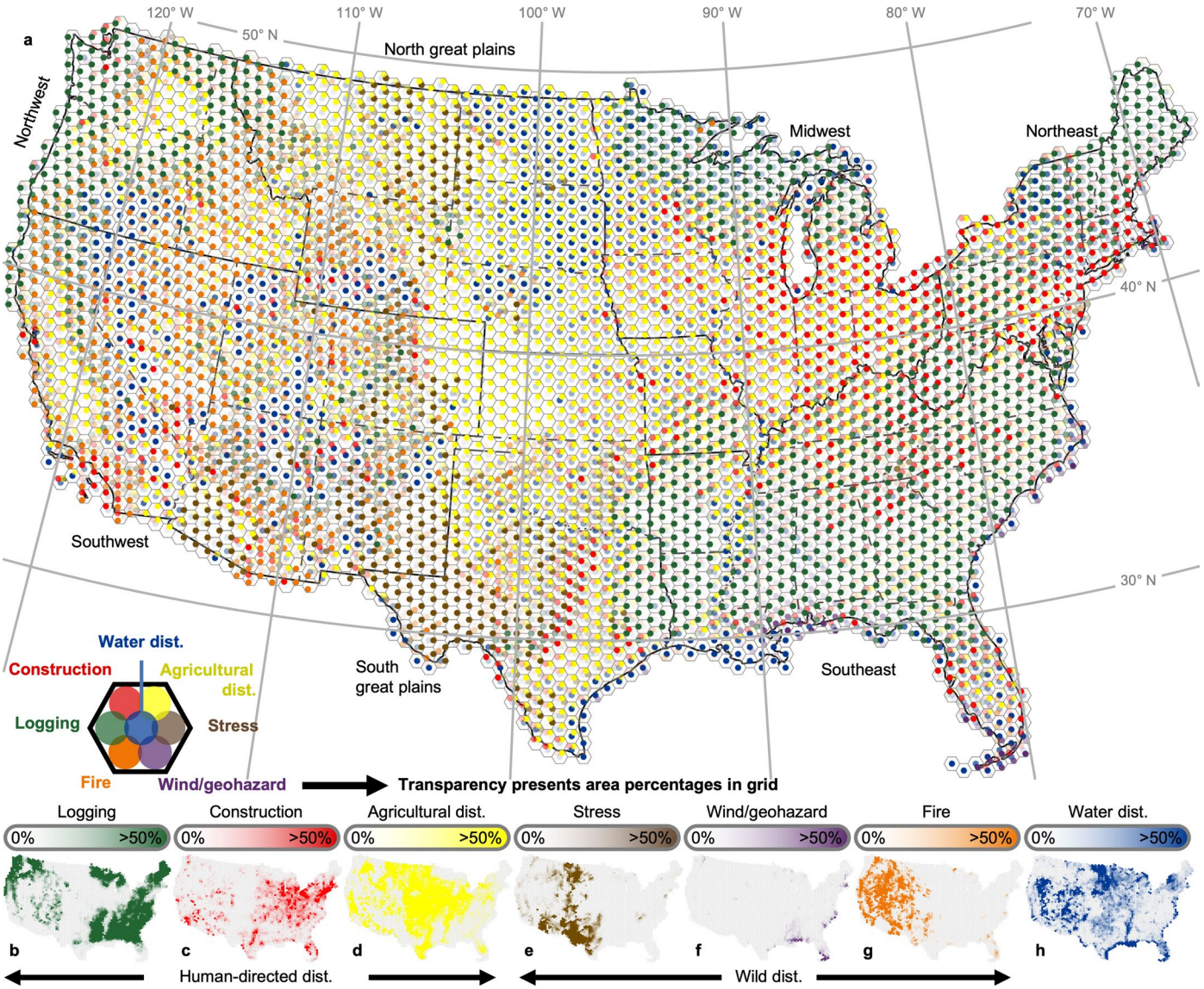

Extended Data Fig. 3 | Distribution of land disturbance agents across the US (1988-2022). a. US-wide map depicting the relative proportion of each disturbance agent's contribution within 2500-km^2 hexagonal grids. Colored points represent agents, with transparency indicating their percentage relative to the seven mapped agents. The predominant agent (>50%) is highlighted within each grid cell. Solid boundaries delineate US Fifth National Climate Assessment regions, while dashed boundaries represent state borders. **b-h.** Area percentage for individual disturbance agents, relative to the seven mapped agents, sharing the same legend as (**a**): (**b**) logging, (**c**) construction, (**d**) agricultural disturbance, (**e**) stress, (**f**) wind/geohazard, (**g**) fire, and (**h**) water disturbance.

https://doi.org/10.1038/s41561-025-01792-3

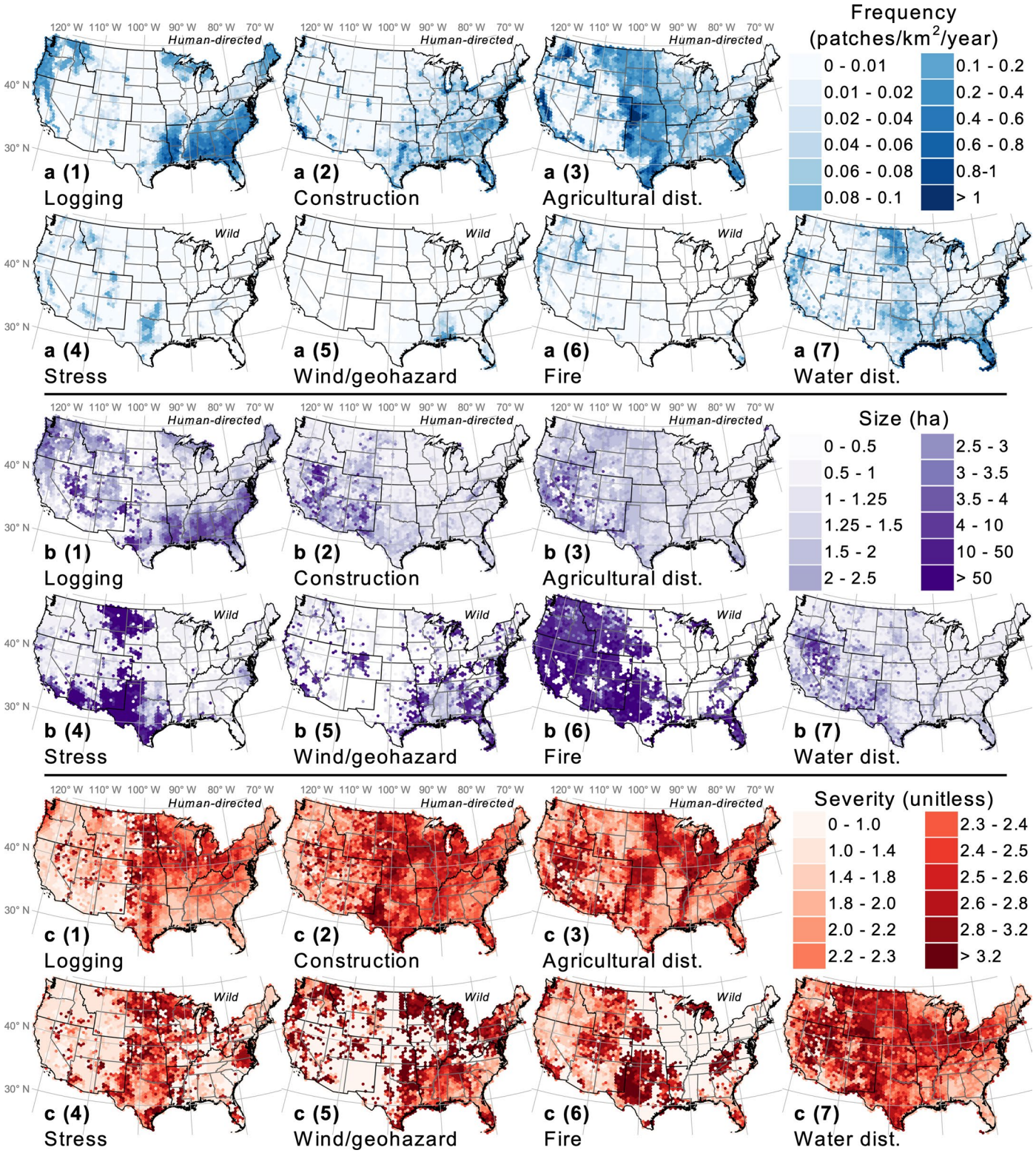

Extended Data Fig. 4 | Land disturbance regimes across the US represented in 2500-km² hexagonal grids (1988-2022). a. Average disturbance patch frequency. **b**. Average disturbance patch size. **c**. Average disturbance patch severity, scaled from 1 to 4, where 0-1 indicates undisturbed to low, 1-2 indicates low to medium, 2-3 indicates medium to high, and 3-4 indicates high to very high. Each panel displays eight maps: (**1**) logging, (**2**) construction, (**3**) agricultural disturbance, (**4**) stress, (**5**) wind/geohazard, (**6**) fire, and (**7**) water disturbance. The black boundaries represent US Fifth National Climate Assessment regions, while the gray boundaries indicate state border. The consistent color scale across all maps facilitates direct comparison of regime characteristics across different disturbance agents. Histograms for each map are provided in Supplementary Fig. 6.

https://doi.org/10.1038/s41561-025-01792-3

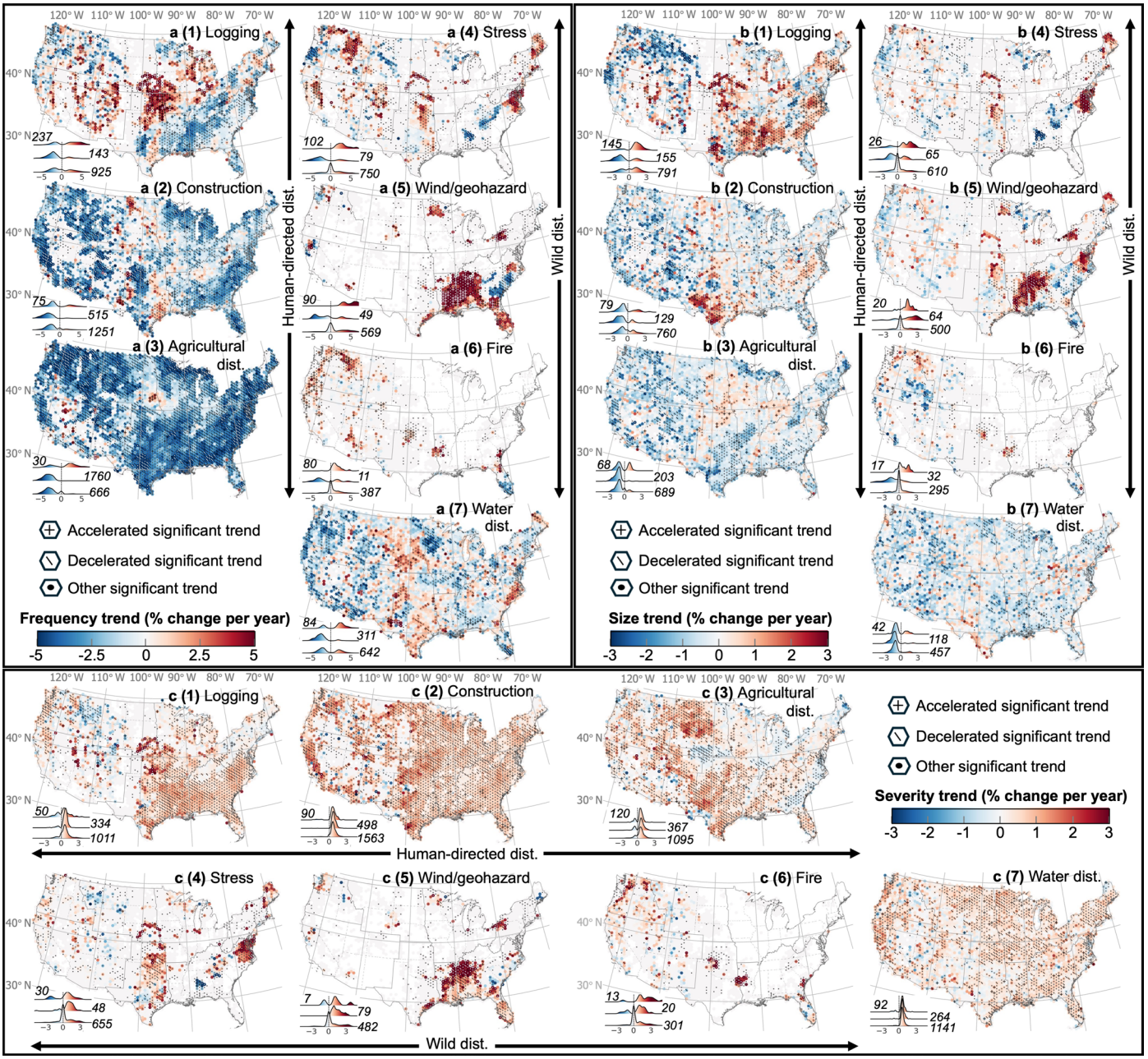

Extended Data Fig. 5 | Map of trend in land disturbance regimes at 2500-km² hexagonal grids across the US (1988-2022). a. Trend of disturbance patch frequency. **b.** Trend of disturbance patch size. **c.** Trend of disturbance patch severity. In each panel, (**1-7**) are the regime trend map of logging, construction, agricultural disturbance, stress, wind/geohazard, fire, and water disturbance. In each map, trends are estimated using the Theil-Sen estimator, and their statistical significance is determined by the two-tailed Mann-Kendall test ($p < 0.05$), where symbols indicate significantly accelerated (+) and decelerated (−) trends, while dots (•) denote other significant (for example, increasing or decreasing) trends. Each map includes density plots in the lower-left corner, depicting the distribution of trend magnitudes for landscapes with significant trends, categorized as accelerated, decelerated, and other significant trends (from top to bottom). The number presents the number of hexagonal grids with significant trend. The solid boundaries represent US Fifth National Climate Assessment regions, while the dashed boundaries indicate state border. The consistent color scale across all maps facilitates direct comparison of disturbance regime shift patterns. All general land disturbance agent regime trends are provided in Fig. 4.